Thermal physics in carbon nanotube growth kinetics

Oleg A. Louchev and Hisao Kanda
Advanced Materials Laboratory, National Institute for Materials Science, 1-1 Namiki, Tsukuba, Ibaraki 305-0044, Japan

Arne Rosén and Kim Bolton
Department of Experimental Physics, School of Engineering Physics, Göteborg University and Chalmers University of Technology, SE-412 96, Gothenburg Sweden

(Received 29 October 2003; accepted 2 April 2004)

The growth of single wall carbon nanotubes (SWNTs) mediated by metal nanoparticles is considered within (i) the surface diffusion growth kinetics model coupled with (ii) a thermal model taking into account heat release of carbon adsorption–desorption on nanotube surface and carbon incorporation into the nanotube wall and (iii) carbon nanotube–inert gas collisional heat exchange. Numerical simulations performed together with analytical estimates reveal various temperature regimes occurring during SWNT growth. During the initial stage, which is characterized by SWNT lengths that are shorter than the surface diffusion length of carbon atoms adsorbed on the SWNT wall, the SWNT temperature remains constant and is significantly higher than that of the ambient gas. After this stage the SWNT temperature decreases towards that of gas and becomes nonuniformly distributed over the length of the SWNT. The rate of SWNT cooling depends on the SWNT–gas collisional energy transfer that, from molecular dynamics simulations, is seen to be efficient only in the SWNT radial direction. The decreasing SWNT temperature may lead to solidification of the catalytic metal nanoparticle terminating SWNT growth or triggering nucleation of a new carbon layer and growth of multiwall carbon nanotubes. © *2004 American Institute of Physics.* [DOI: 10.1063/1.1755662]

I. INTRODUCTION

The growth of carbon nanotubes is a complicated process involving many different phenomena and effects that determine the nanotube's structural and physical properties.[1–23] For example, changes in temperature significantly affects carbon nanotube (NT) nucleation,[24–30] post-nucleation assembly of intermediate carbon structures[30,31] growth rate and carbon NT length,[32,33] transition from single wall NT (SWNT) growth to multiwall NT (MWNT) growth,[34,35] metal catalyst nanoparticle behavior, etc.[16,33,36–38] However, precise control of the growth temperature is only possible in chemical vapor deposition methods where the temperature of the growing tube is the same as that of the substrate and, in addition, this temperature control exists only when the carbon NT forest remains shorter than the characteristic carbon NT heat conductance length.[33] In other growth processes, such as arc discharge and laser ablation synthesis, the growth of carbon NTs and the growth temperature is defined by a complicated process involving many effects characterized by different time and length scales related to surface phenomena (adsorption/desorption, surface diffusion, catalysis),[39–42] gas-NT heat exchange processes,[43,44] evaporation kinetics of the metal-graphite target,[13,17,18,22] carbon vapor and buffer gas flow dynamics coupled with carbon condensation, heat and mass transfer,[17–20,22,45,46] plasma and related electric field effects.[13]

Thus, on the one hand the carbon NT growth process includes microkinetics processes[39–44,47–57] described by quantum mechanical approximations and empirical interatomic potentials,[58–61] giving characteristic energies and activation energy barriers which determine kinetic pathways of carbon nanostructure assembly. On the other hand, the growth kinetics also depends on macroscopic parameters such as carbon vapor pressure, inert gas pressure and temperature, etc., which may be modeled by classical continuum formalisms of gas flow dynamics coupled with heat and mass transport. Nevertheless, a combined description of carbon NT growth kinetics requires an additional model which combines both microscopic, nanoscale processes with macroscopic processes related to the different growth techniques.

In this paper we develop a thermokinetic model for the growth of an individual carbon NT in the vapor. The model includes microscopic parameters provided by atomistic models, as well as macroscopic parameters derived from continuum models of evaporation, gas flow dynamics, heat and mass transfer. In particular, we consider a model for a growing carbon NT experiencing C vapor condensation and heat exchange with chemically inert gases (He, Ne, Ar, and Xe). This model integrates (i) carbon NT growth kinetics within the framework of the continuum surface diffusion approximation,[32,33] (ii) microenergetics obtained from atomic-level calculations,[39–42] (iii) phenomenological approximations for thermal processes of carbon condensation heat release and heat dissipation rates[31,33] and (iv) molecular dynamics simulations of the heat exchange between carbon NTs and ambient inert gases.[43,44] Numerical calculations and analytic approximations based on this combined multiscale model reveal significant properties of SWNT growth.

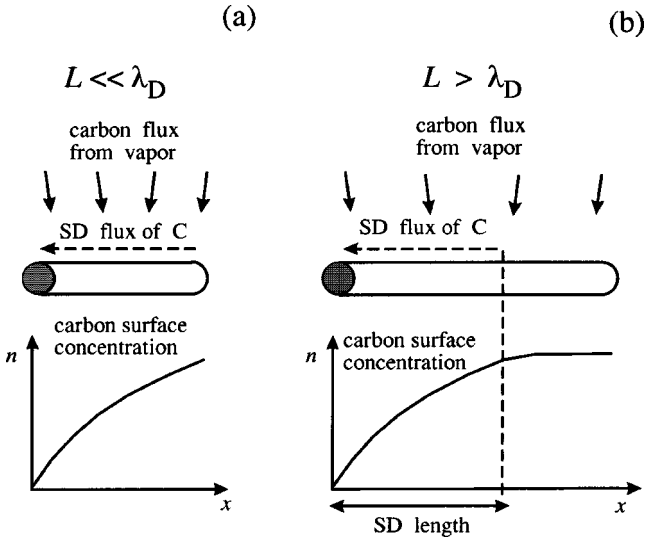

FIG. 1. Illustration of the model presented in this work for short SWNTs [$L \ll \lambda_D$, panel (a)] and long SWNTs [$L > \lambda_D$, panel (b)].

II. SWNT GROWTH MODEL

A. Growth kinetics and the thermal model

In this paper we consider the catalyzed growth of a SWNT mediated by surface diffusion of carbon atoms along the outer SWNT wall as illustrated in Fig. 1. The catalytic metal particle, which is attached to the SWNT end, is shown as a gray sphere in the figure. It is assumed that the main role of metal nanoparticle is to prevent closure of the SWNT end.[31–33] This model is not restricted to a specific mechanism of SWNT nucleation, but assumes that nucleation may occur by any of several possible pathways such as carbon precipitation from metal-carbon nanoparticles, from semifullerene carbon clusters, or by graphitic nanofragment interaction with metal nanoparticles.[26–30] Irrespective of the nucleation mechanism, our model considers the postnucleation stage and relevant kinetics processes when the SWNT length, L, which is initially much smaller than the characteristic surface diffusion length, λ_D [Fig. 1(a)], increases with time [Fig. 1(b)]. In considering this problem we assume that the growth of SWNTs is fed by carbon atoms that initially adsorb onto the SWNT surface and then diffuse to the tube end where the metal nanoparticle is attached. At this stage the adsorbed atom is incorporated into the growth edge (via the metal catalyst) and finally forms part of the hexagonal SWNT network. This assumption is based on several atomistic microenegetic studies[39,41,42] giving adsorption energy and activation energy for surface diffusion, and which all suggest that the adsorbed carbon atoms are able to migrate over micron distances along carbon NT surfaces to reach the open ends where they are incorporated into the growing SWNT structure. Although carbon atoms may impinge onto both the metal nanoparticle and the lateral SWNT surface, when formulating the postnuleation growth problem for SWNT lengths much larger than the metal nanoparticle (and SWNT) diameter, we assume that the contribution of the SD flux over the lateral surface dominates over the diffusion through the surface of metal particle. Therefore, we assume that the growth rate is controlled by SD over the SWNT surface. In addition to the restrictions described above, the model considers carbon atoms, for which the adsorption and surface diffusion activation energies are known from quantum mechanical calculations.[39,41,42] In fact, under experimental conditions there may also be contributions from other carbon species in the supersaturated vapor.[15] We assume that (i) carbon atoms dominate in SWNT formation or (ii) other carbon species impinging onto SWNT surface also have high surface mobility. If this assumption were not correct then SWNT formation would not be possible since low mobility carbon clusters on the SWNT surface would be effective aggregation centers leading to the formation of outer graphite layers and hence to MWNT formation.

Although an exact solution for carbon atom migration over carbon NTs has been derived in a recent study,[62] we use a phenomenological continuum approximation which can easily be coupled with the related thermal phenomena of the SWNT growth. The model described above yields the following distribution of carbon atom concentrations over the SWNT surface:

$$\partial n/\partial t + \nabla J_s = Q_c - n/\tau_a, \tag{1}$$

where Q_c is the impinging carbon flux onto SWNT surface from the vapor, $\tau_a \approx \upsilon^{-1} \exp(E_a/k_BT)$ is the adsorption time ($\nu \approx 10^{13}$ Hz is the thermal vibration frequency and $E_a \approx 1.8-3.6$ eV is the adsorption energy depending on the SWNT radius and chirality,[39,41,42] and J_s is the SD flux of carbon expressed via the chemical potential of the C adsorbate as

$$J_s = -\frac{nD_s}{k_BT}\,\mathrm{grad}\,\mu = -D_s\,\mathrm{grad}\,n + nD_s \ln(n/n_0)T^{-1}\,\mathrm{grad}\,T, \tag{2}$$

where $D_s = a_0^2 \nu \exp(-\delta E_d/k_BT)$ is the SD coefficient including the activation energy of surface diffusion, $\delta E_d \approx 0.2-1.5$ eV[39,41,42] and n_0 is the surface density of adsorption sites (this expression is correct only for $n/n_0 \ll 1$).

The problem is solved using the following boundary condition at the SWNT growth edge ($x=0$):

$$kn = -J_s, \tag{3}$$

where $k = k_0 \exp(-\Delta E/k_BT)$ is the Arrhenius-type kinetic constant for incorporation of C atoms into SWNT wall with specific activation energy barrier ΔE (defined for NT growth in Refs. 31 and 32). At the opposite end of the SWNT we assume $J_s = 0$.

The SWNT growth rate is

$$V = dL/dt = \Omega J_s|_{x=0}, \tag{4}$$

where Ω is the specific area per one carbon atom in SWNT wall.

Experimental studies[6,22,23] have shown that the growth of SWNTs by arc discharge and laser ablation techniques takes place only in the presence of inert gases under pressures higher than 10^4 Pa. In previous papers[30,31] it has been suggested that the inert gas facilitates effective dissipation of the heat that is released during carbon NT nucleation and growth. Effective heat dissipation is necessary since the in-

crease in tube temperature caused by this heat release ($E_b \approx 7.3$ eV per atom) would lead to disintegration of the SWNTs.

The heat release due to carbon condensation into SWNTs, $E_b \approx 7.3$ eV (Ref. 63) can be divided into two steps: (i) adsorption heat release when the C atom chemisorbs on the SWNT surface (E_a) per atom times the carbon impingement rate (Q_c), and (ii) the heat release at the SWNT growth edge in contact with metal particle where carbon atoms are incorporated into the SWNT structure ($E_{\text{inc}}=E_b-E_a$) times the carbon flux at SWNT edge (J_s). The adsorption heat release over the SWNT surface, $Q_c E_a$, is partially compensated for by heat dissipation due to carbon desorption, i.e., $E_a n/\tau_a$. The remaining mechanisms of heat dissipation from the SWNT surface are radiation and collisions with chemically inert gases.

For short SWNTs the nonuniformity of the heat release over the length of the SWNT (which is larger at the end where C atoms are incorporated into the tube structure) is smoothed out by heat conduction along the SWNT. However, when the length of the SWNT approaches the heat conduction length,[33] the temperature distribution along the SWNT becomes nonuniform. This necessitates the application of models which allow one to define a temperature field (T field) along the SWNT. In this work we evaluate temperature regimes of the growing SWNT and its effect on growth kinetics based on the continuum differential equation for thermally thin shells including surface adsorption heat release and dissipation rates in the form of the equivalent sources and sinks of heat,

$$\rho c\, \partial T/\partial t + \nabla J_T = \frac{1}{\delta}\{E_a(Q_c - n/\tau_a) - q_d\}, \tag{5}$$

where $\delta \cong 0.2$ nm is the wall thickness, q_d is the heat dissipation function defined below and $J_T = -k_s(T)\,\text{grad}\,T$ is the conduction heat flux along the SWNT wall. The heat conductance is taken from data obtained for graphite along the basal plane[64] and is approximated as $k_s(T) = 118\exp(1500/T)$ W/m K for $T = 1000-2000$ K.

The carbon condensation heat release that is due to C atom inclusion in the tube structure ($E_{\text{inc}}=E_b-E_a$) and which occurs at the growth edge, is taken into account by the boundary condition at this edge ($x=0$):

$$k_s\,\text{grad}\,T = (E_b - E_a)J_s/\delta. \tag{6}$$

At the opposite end of SWNT ($x=L$) we assume that $\text{grad}\,T=0$. As mentioned above, we consider only those stages when the SWNT is much longer than the metal particle diameter, and thus heat provided by carbon impinging onto this nanoparticle as well as heat dissipation from its surface are assumed to be negligibly small compared with the thermal effect of carbon impinging onto the SWNT wall.

The thermokinetic model given above describes a coupled behavior of the system where the parameters of growth kinetics problem (D_s, τ_a, J_s, and k_{inc}) are defined by the T-field distribution, and the concentration distribution and resulting J_s at the growth edge defines the T field.

B. SWNT–ambient gas heat exchange

The heat dissipation term, q_d, in Eq. (5) includes heat loss by radiation and by collisions with chemically inert carrier gases. Several experimental studies show that SWNTs form at high inert gas pressures 10^4-10^5 Pa,[6,22,23] where the contribution of radiative heat loss may be neglected. Thus, in this work we assume that the condensation heat dissipates solely by collisions with the ambient inert gas.

Heat dissipation from the SWNT that is due to collisions with gas atoms is equal to the energy transferred from the SWNT per collision, ΔE_k, multiplied by the flux of colliding atoms per surface area unit, Q_g. That is $q_d = \Delta E_k Q_g$ where $Q_g = P_g/(2\pi m_g k_B T_g)^{1/2}$ and P_g is the gas pressure, m_g is the mass of the gas atoms and T_g is the gas temperature. One of the simplest approximations for the collisional energy transfer, ΔE_k, is the strong collision assumption (SCA).[65] This assumes that the temperature of the gas atom after the collision is the same as the tube temperature, T. Hence, since the gas atom has three translational degrees of freedom, according to the equipartition principle its energy after the collision is $3/2k_BT$. The energy transferred over the collision is merely the difference between this energy and the gas atom energy before the collision, $3/2k_BT_g$. Hence, $\Delta E_k = 3/2k_B(T-T_g)$.

However, the SCA usually overestimates collisional energy transfer,[66] and hence an accommodation factor, $0<\alpha<1$, is included in the expression for the collisional energy transfer, i.e., $\Delta E_k = 3/2\alpha k_B(T-T_g)$ and accordingly

$$q_d = \tfrac{3}{2}\alpha Q_g k_B(T-T_g) = h_g(T-T_g), \tag{7}$$

where $h_g = 3\alpha Q_g k_B/2$ is the heat exchange coefficient. Much progress has been made towards determining α solely from theoretical considerations (e.g., ergodic collision theory and its successors),[66] but obtaining the correct input for these theories makes *a priori* prediction very difficult. For example, many of these theories require an effective number of reactant and gas molecule degrees of freedom that couple strongly during the collision and hence lead to a local statistical sharing of energy.[66]

Similarly to these models, we assume that collisional energy transfer is linearly dependent on the initial and final energies of the gas molecule [i.e., $\Delta E_k \propto 3k_B(T-T_g)/2$]. However, we use results obtained from molecular dynamics simulations of inert gas atoms with SWNTs[43] to estimate the functional form and magnitude of the accommodation coefficient, α. Two features that are clearly evident from the simulations are that (i) the amount of collisional energy transfer depends on the mass of the colliding gas and (ii) there is substantial energy transfer in the tube radial direction and negligible energy transfer in the tube circumferential and axial directions.

Figure 2 is a ln–ln plot of $\langle \Delta E_{\text{tot}} \rangle$ and $\langle \Delta E_{\text{rad}} \rangle$ versus m_g, where $\langle \Delta E_{\text{tot}} \rangle$ is the total collisional energy transfer between the colliding inert gas and the NT averaged over all collisions, $\langle \Delta E_{\text{rad}} \rangle$ is the associated energy transfer in the radial direction only, and m_g is the mass of the colliding gas (He, Ne, and Xe). The tube temperature was 1300 K, the initial relative translational energy between the gas atom and

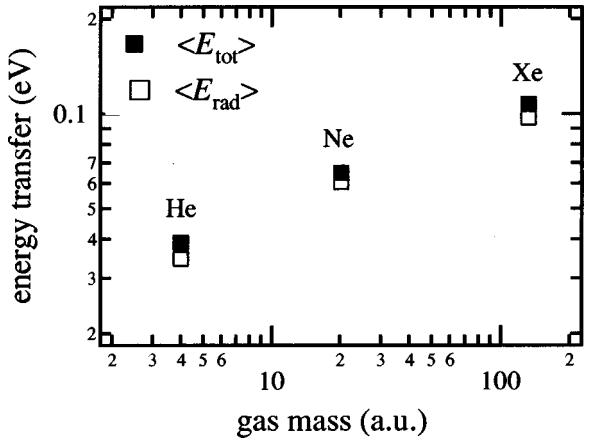

FIG. 2. Molecular dynamics results of energy transfer in SWNT–inert gas collisions.

the tube was 0.06 eV, and the in-plane incident angle was 45°. It is evident that the total energy transfer is dependent on the gas mass, which should therefore be included in the accommodation coefficient. Also, the slope of this ln–ln curve is $\approx 1/3$, so that α should include a factor $(m_g/m_{\mathrm{ref}})^{1/3}$. The reference mass, m_{ref}, is included to obtain a dimensionless accommodation coefficient, and since this work (and the simulations) considered inert gas atoms only, we choose the reference mass to be that of the heaviest inert gas studied, Xe (131.3 a.u.).

The features of the energy transfer seen in Fig. 2 are also observed at other carbon NT temperatures, collision energies, and incident angles. However, only collisions with a (10,0) SWNT were studied, and since the $(m_g/m_{\mathrm{ref}})^{1/3}$ dependence may not be general for all tubes (for example, the restoring force in the NT's radial direction—which plays a key role in energy transfer—varies with NT diameter), we also investigate the sensitivity of this functional dependence on the growth kinetics. In particular, the simulations revealed that the vast majority of inert gas—nanotube collisions have only one encounter and that, during this single encounter, there is very efficient energy transfer. As discussed in the previous paper,[43] the collision mechanism may best be described as impulsive and leading to large energy transfer. According to the simple Baule formula[67] for impulsive collisional energy transfer, $\Delta E_k=[4\mu/(1+\mu)^2]E_i$, where E_i is the initial energy of the colliding gas atom and $\mu=m_g/M_{\mathrm{eff}}$ is a reduced mass that is the ratio of the gas mass, m_g, to the effective SWNT mass, M_{eff}. It is important to note that this effective mass includes many hidden physical properties, such as the rate of energy flow from the collision center and the efficiency with which energy is exchanged between the gas atom and the SWNT. In fact, the simulations showed that the gas–SWNT collisions caused radial indentation of the tube at the collision center (since the radial forces are weak). This resulted in the larger energy transfer—particularly in the radial direction—seen in Fig. 2. Hence, the effective mass of the SWNT is not sensitive to the tube length (since indentation is localized to the collision center) and it is small (i.e., it is the mass of the collision center which has weak radial restoring forces). We thus use a small effective mass in the Baule formula since this yields the efficient energy transfer seen in the simulations. The limit for efficient energy transfer is when $m_g=M_{\mathrm{eff}}$ and $\Delta E_k=E_i$, so that energy transfer is proportional to the gas mass. Hence, we also test a linear dependence of m_g/m_{ref} in the accommodation coefficient.

Figure 2 also shows that the total and radial energy transfers are very similar. Simulations showed that the total energy transfer is dominated by transfer in the radial direction under all conditions studied, and that transfer in the circumferential and axial tube direction is insignificant. Hence, only one gas translational degree of freedom is involved in the collisional energy transfer, so that ΔE_k is proportional to $k_B(T-T_g)/2$ and not $3k_B(T-T_g)/2$ as in the strong collision assumption. The accommodation coefficient should accordingly have a factor 1/3.

Based on these results, two approximations for α are considered, i.e.,

$$\alpha=1/3\beta(m_g/m_{\mathrm{ref}})^n, \tag{8}$$

where $n=1/3$ or $n=1$. As discussed above, m_{ref} is xenon's mass and $0<\beta<1$ is a factor that may be included if energy transfer in the radial direction is much less than the strong collision assumption. In fact, the molecular dynamics simulations of Xe collisions with SWNTs show that the radial component of the Xe energy is essentially thermalized to the tube temperature after collision (i.e., $\beta=1$). However, as mentioned above, the simulated collisions are head-on (the out-of-plane impact parameter is zero) and glancing collisions may have lower collisional energy transfer. In this work we test the significance of this β parameter on the SWNT growth mechanisms.

III. RESULTS AND DISCUSSION

A. Temperature variations during SWNT growth

The problem defined by Eqs. (1)–(8) was solved numerically by an adaptive finite-difference scheme using iterations to take into account all nonlinearities between the growth kinetics [Eqs. (1)–(4)] and the thermal physics contributions [Eqs. (5)–(7)]. We consider regimes where all macroscopic parameters such as the carbon vapor pressure, gas pressure, and gas temperature are assumed to be constant over time. However, even for these simplified conditions the model exhibits complex behavior revealing a number of significant issues for understanding carbon NT formation. Although recent data[41,42] shows larger values for the adsorption energy E_a and the activation energy for surface diffusion δE_d, we use microenergetic data of Ref. 39 for the simulations reported here. Notwithstanding the differences between the used here values[39] and more recent values,[41,24] for all illustrative cases discussed below, where SD lengths obtained from both sets of values are similar, the results from the thermo-kinetical model using either the two data sets give quantitative agreement.

Figure 3 shows typical results obtained from the simulation of SWNT growth, giving the dependencies of (a) SWNT length, (b) growth rate, and (c) SWNT temperature over time. T_{max} is the temperature of the tube at $x=0$ (the growth edge) and T_{min} is the temperature at $x=L$ (the end of the

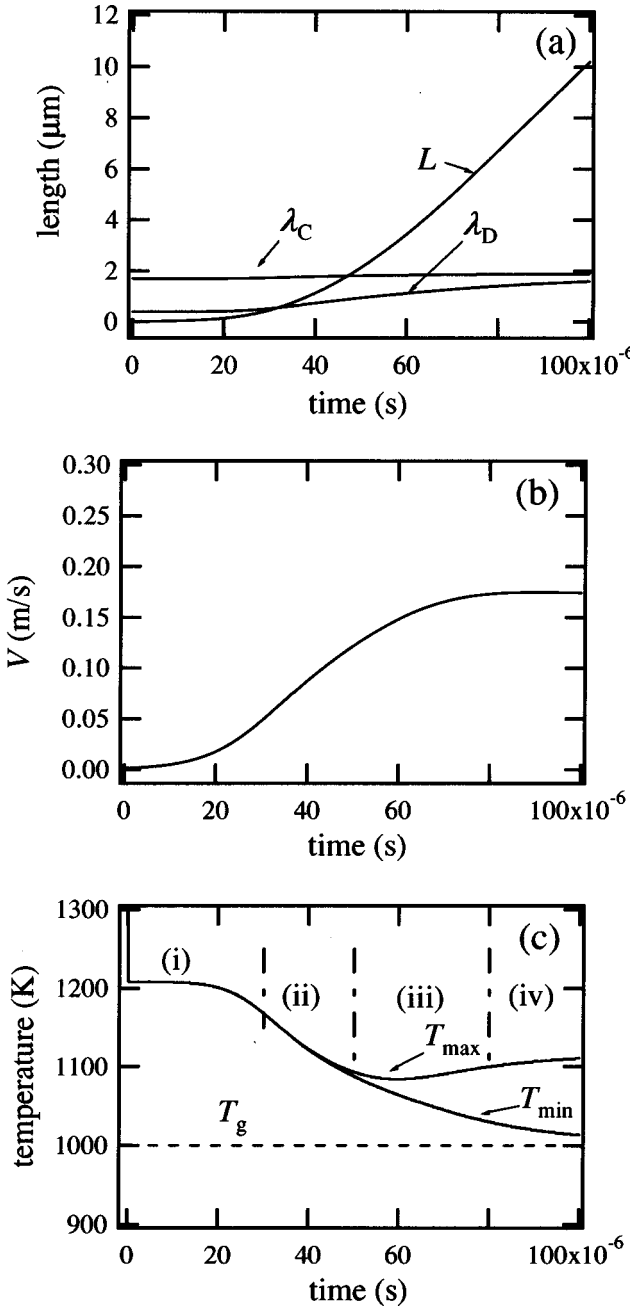

FIG. 3. Typical simulation results obtained from the model defined by Eqs. (1)–(8) showing (a) SWNT length together with SD length, Eq. (9), and heat conductance length Eq. (10), (b) SWNT growth rate, and (c) the maximum and minimum temperatures along the SWNT.

tube where there is no growth). The results are for a carbon vapor pressure $P_c \approx 200\,\mathrm{Pa}$ and for He at $P_g = 10^5\,\mathrm{Pa}$ and $T_g = 1000\,\mathrm{K}$. The thermal accommodation coefficient in this simulation is $\alpha = 1/3$, which corresponds to the maximal possible heat dissipation rate (due to radial energy transfer, see Sec. II B). First, these figures show even for maximal value of α that the SWNT temperature may differ significantly from that of the ambient gas, and that the temperature of the SWNT does not equilibrate with the gas due to continued heat release from condensation of the carbon vapor. In particular, for the conditions considered in Fig. 3, the temperature is shown to be more than 200 K in excess of $T_g = 1000\,\mathrm{K}$. Moreover, the SWNT temperature has a complicated behavior over time, going through various stages after the temperature drops from the initial value: (i) first, the SWNT temperature remains constant and is uniformly distributed over the SWNT length, (ii) then the SWNT temperature decreases but still remains uniformly distributed along the SWNT, (iii) SWNT temperature nonuniformity appears, and (iv) finally the growth rate and the temperature gradient along the SWNT stabilizes.

These stages are due to the two characteristic length scales of the SWNT growth. The first is the surface diffusion length λ_D defined by

$$\lambda_D \approx \sqrt{D_s \tau_a}, \tag{9}$$

which characterizes the length which carbon adatoms can travel over the surface prior to their desorption.

The second is the heat conductance length given by

$$\lambda_C \approx \sqrt{k_s \delta / h_g}. \tag{10}$$

This length characterizes the length which heat can effectively distribute along the SWNT shell by heat conductance (k_s) when there is heat exchange with the ambient gas (h_g).

Both of these lengths are shown in Fig. 3(a) as a function of time. They are estimated from the average SWNT temperature corresponding to the actual simulation time, and are shown together with the value of SWNT length. Comparison of these lengths with the SWNT length suggests that the transition from the first to the second temperature stage [see (i) and (ii) in Fig. 3(c)] occurs when the SWNT length is similar to the SD length ($L \approx \lambda_D$) and the transition from the second to the third stage occurs when SWNT length is similar to the heat conductance length ($L \approx \lambda_c$).

Thus, the first stage, which is characterized by a constant SWNT temperature, is when $L < \lambda_D$, i.e., when all adatoms diffuse to the SWNT edge and are incorporated into the wall. That is, all atoms impinging onto the SWNT wall contribute to the heat release by an amount that equals the binding energy ($E_b = 7.3\,\mathrm{eV}$ per atom which, as discussed above, is released in two steps). Thus, during this stage, the heat release of carbon condensation, $\approx 2\pi R L Q_c E_b$, and the heat dissipation to the ambient gas, $\approx 2\pi R L h_g (T - T_g)$, are both proportional to the SWNT length, L. Considering this balance and taking into account the expression for h_g [Eq. (7)] one finds an explicit analytical estimate for the SWNT temperature during this stage,

$$T - T_g \approx \frac{Q_c E_b}{h_g} \approx \frac{2}{3} \frac{E_b P_c}{\alpha k_B P_g} \frac{m_g^{1/2}}{m_c^{1/2}}. \tag{11}$$

Irrespective of the initial cluster temperature ($T_{\mathrm{in}} = 1500\,\mathrm{K}$), the SWNT temperature stabilizes during this stage with a characteristic time of order $\tau^* \approx m_c C/(S_a h_g)$, where m_c is the atomic mass of carbon and S_a is the specific area per atom in the SWNT wall. For $C = 2\,\mathrm{kJ/kg\,K}$, $h_g = 2.85 \times 10^4\,\mathrm{W/m^2\,K}$ and $S_a = 2.62 \times 10^{-20}\,\mathrm{m^2}$ one obtains $\tau^* \approx 5 \times 10^{-7}\,\mathrm{s}$. The end of this temperature stage occurs when $L \approx \lambda_D$ [see Fig. 3(a)], which can be calculated by inserting the value of T defined in Eq. (11) into Eq. (9).

When the SWNT becomes longer than the SD length, only those C atoms that impinge onto the SWNT surface within the SD length from the growth edge can reach the edge before desorption [see Fig. 2(b)]. C atoms impinging outside this length desorb back into gas and do not contribute to the heat release (for these atoms the adsorption heat is exactly compensated for by the desorption heat). Therefore, during this stage heat release of condensation is proportional to the SD length, $2\pi R\lambda_D Q_c E_b$, whereas the heat dissipation is still proportional to the total SWNT length $2\pi RLh_g(T-T_g)$. The balance gives the following analytical estimate for SWNT temperature during this stage:

$$T-T_g=\frac{Q_cE_b}{h_g}\frac{\lambda_D}{L}\approx\frac{2}{3}\frac{E_bP_c}{\alpha k_BP_g}\frac{m_g^{1/2}}{m_c^{1/2}}\frac{\lambda_D}{L}, \tag{12}$$

Eq. (12) explicitly shows the decrease in T with increasing L [as seen in stage (ii) in Fig. 3(c)].

Figure 3(c) shows that during the first and second stages the temperature remains uniform along the SWNT (i.e., $T_{\max}\approx T_{\min}$). This is because the heat flux released near the edge ($\propto E_a$), and directly at the edge ($\propto E_b-E_a$), is able to redistribute along the entire SWNT. A temperature gradient appears during the third stage, which begins when $L\geqslant\lambda_C$. In fact, our simulations show that for many conditions the third stage does not appear even when the SWNT becomes longer than λ_C. Under these conditions the third stage occurs when-the-SWNT temperature is very close to T_g before L becomes longer than λ_C. Typical results showing this behavior are presented in Fig. 4, and are obtained for $P_c\approx 200$ Pa, $P_g=10^5$ Pa (He and $\alpha=1/3$) and $T_g=1200$ K. In particular, this figure shows that when SWNT length is $L\approx\lambda_C$ [Fig. 4(a)] its temperature is very close to T_g, and the final temperature difference along the SWNT, $T_{\max}-T_{\min}\approx 5$ K, is insignificant. One can estimate whether the third and fourth stages shown in Fig. 3(c) will occur for a given set of parameters by substituting $L=\lambda_C$ in Eq. (12) and determining the value of $T-T_g$ when the temperature nonuniformity appears.

When the temperature distribution along the SWNT remains uniform, as in Fig. 4, the model defined by Eqs. (1)–(8) may be reduced to a significantly simpler approximation. First, for a uniform temperature distribution Eqs. (1)–(4) allow a quasisteady state solution for the SWNT growth rate,

$$\frac{dL}{dt}=-\Omega D_s\frac{dn}{dt}=\frac{\Omega kQ_c\tau_a\sinh(L/\lambda_D)}{\sinh(L/\lambda_D)+(k\lambda_D/D_s)\cosh(L/\lambda_D)}, \tag{13}$$

which depends on the temperature.

Second, when the temperature along the SWNT is uniform Eqs. (5)–(7) reduce to a simpler approximation. Integration of Eq. (5) over the entire SWNT surface, and application of Gauss theorem, allows one to substitute $\int\nabla^2T\,dS$ by the value of ∇T at the boundaries (i.e., at $x=0$ and $x=L$). This yields the following equation for the SWNT temperature:

$$Mc\frac{dT}{dt}=2\pi R\int_0^L E_b[Q_c-n(x)/\tau_a]dx - 2\pi RLh_g(T-T_g), \tag{14}$$

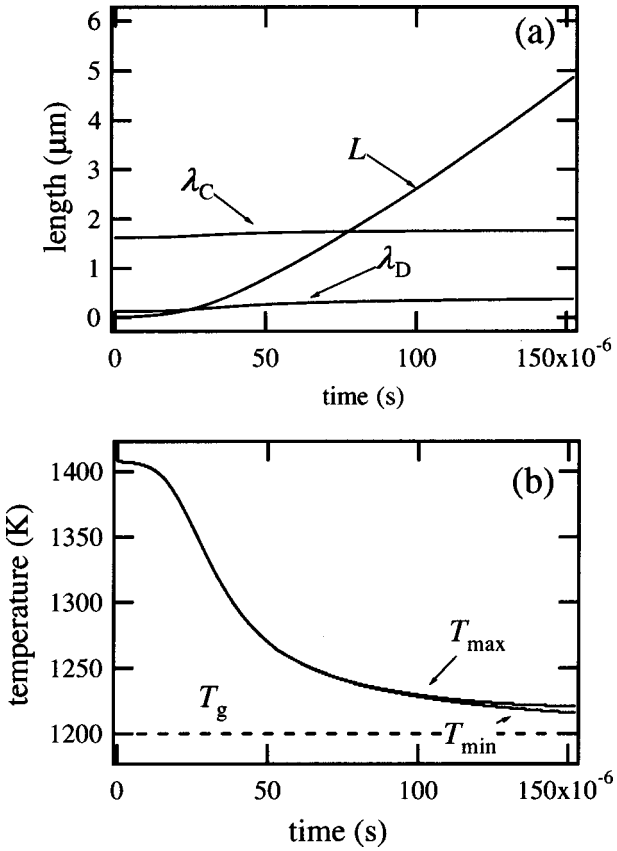

FIG. 4. Simulation of the model defined by Eqs. (1)–(8) showing (a) SWNT length together with SD length, Eq. (8), and heat conductance length, Eq. (11), (b) the maximal and minimal temperature of SWNT. In contrast to Fig. 3 the difference in the maximum and minimum tube temperatures ($T_{\max}-T_{\min}$) is very small and occurs when $L\gg\lambda_C$.

where M is the SWNT mass and $n(x)=Q_c\tau_a+C_1\times\exp(-x/\lambda_D)+C_2\exp(x/\lambda_D)$ is the surface concentration distribution of the adsorbed carbon on the SWNT.

By determining the integration constants C_1 and C_2 from the boundary condition for the adsorbed C atom concentration field, and using $M\approx m_cN$ and $2\pi RL\approx S_aN$ (where S_a is specific surface per atom and N number of atoms in the wall) one obtains the following approximation for the SWNT temperature:

$$\frac{dT}{dt}=\frac{S_a}{m_cC}\{E_bQ_ck\tau_aU^*L^{-1}-h_g(T-T_g)\}, \tag{15}$$

where U^* is a dimensionless parameter dependent on the SWNT length as

$$U^*=\frac{\exp(L/\lambda_D)-1+\exp(2L/\lambda_D)[1-\exp(-L/\lambda_D)]}{[1+\exp(2L/\lambda_D)]k\lambda_D/D_s-[1-\exp(2L/\lambda_D)]}. \tag{16}$$

Hence, when the temperature is uniformly distributed along the SWNT (restricted by the condition $L<\lambda_C$) the simplification given by the set of two ordinary differential equations (13) and (15) is valid, provided that the characteristic times of the adjustment of the concentration and temperature fields, given by L^2/D_s and $L^2\rho C/k_s$, respectively, are much smaller than the characteristic time of SWNT growth, i.e., $L(dL/dt)^{-1}$.

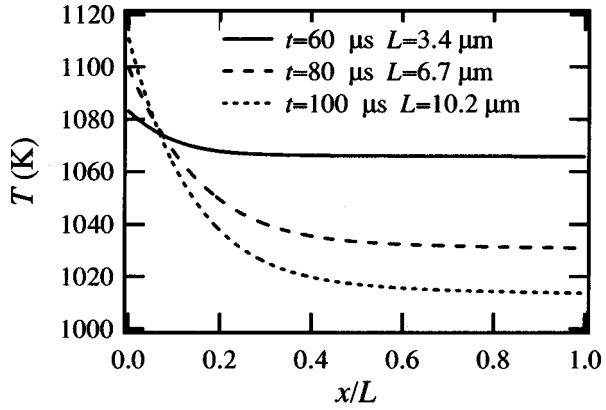

FIG. 5. Temperature distributions along the SWNT for stages (iii) and (iv) shown in Fig. 3(c).

As discussed above, a significant temperature gradient along the SWNT appears with increasing L only when (for $L \approx \lambda_C$) the temperature is not similar to T_g. During stage (iii) this gradient increases whereas during stage (iv) it stabilizes as shown in Fig. 3(c). Figure 5 shows the temperature distributions along the SWNT as a function of a nondimensional coordinate x/L for time $t=60\,\mu$s [stage (iii) when $L \approx 3.4\,\mu$m and is close to $\lambda_C \approx 1.83\,\mu$m], $t=80\,\mu$s [stage (iii) when $L \approx 6.7\,\mu\text{m} > \lambda_C \approx 1.87\,\mu$m] and $t=100\,\mu$s [stage (iv) when $L \approx 10.2\,\mu\text{m} \gg \lambda_C \approx 1.89\,\mu$m]. Figures 3(c) and 5 show that the maximum temperature, $T_{\max}=T(x=0)$, increases with increasing L. This is due to the increase in λ_D occuring with decreasing SWNT temperature (since atoms remain adsorbed on the SWNT surface for longer times at lower temperatures) which leads to more carbon being incorporated into the SWNT structure at the tube edge, and hence an increase in the growth rate and heat release at $x=0$. For example, starting at the end of the second stage ($t \approx 50\,\mu$s) $T \approx 1100$ K and $\lambda_D \approx 0.94\,\mu$m, the temperature far from the growth edge [$T_{\min}$ in Fig. 3(c)] decreases towards $T=1000$ K and leads to increase in the SD length to $\lambda_D \approx 1.6\,\mu$m.

Stabilization of the temperature gradient along the SWNT—during stage (iv) in Fig. 3(c)—occurs when the SWNT length is $L \gg \lambda_C$. During this stage $T_{\min}$ tends to T_g whereas $T_{\max}$ tends to a value for which an analytical approximation can be obtained if $T_{\max}$ is not far from T_g and all nonlinearities in Eqs. (1)–(7) are neglected. In this case, assuming that (i) $T(x)$ is close to T_g and $J_s = -D_s(T_g)dn/dx$, and (ii) the fields of $T(x)$ and $n(x)$ are steady state, one finds for $T_{\max}=T(0)$,

$$T_{\max}-T_g=\frac{(E_b-E_a)\lambda_C}{\Omega\,\delta k_s(T_g)}\frac{dL}{dt}+\frac{E_aQ_c}{h_g(1+\lambda_C/\lambda_D)}\frac{k\lambda_D/D_s}{1+k\lambda_D/D_s}, \tag{17}$$

where the growth rate is

$$\frac{dL}{dt}\approx\frac{\Omega k Q_c\tau_a}{1+k\lambda_D/D_s}, \tag{18}$$

which yields $dL/dt \approx \Omega Q_c \lambda_D$ for $k\lambda_D/D_s \gg 1$.

The first term in Eq. (17) describes the heat release at the growth edge and the second term is for the adsorption heat release over the SD length. As an example, we use these equations for the following set of parameters: $T_g=1000$ K, $E_b=7.3$ eV, $E_a=1.78$ eV, $\Omega=2.62\times10^{-20}$ m^2, $\delta=0.2$ nm, $P_c=200$ Pa and $Q_c=5.07\times10^{24}$ l/m^2 s, $h_g=2.85\times10^4$ W/m^2 K, $\lambda_c=1.9\times10^{-6}$ m, $\lambda_D=1.74\times10^{-6}$ m, $k=9.4\times10^2$ m/s, $k_s=5.3\times10^2$ W/m K, $D_s=1.3\times10^{-7}$ m^2/s. For these parameters one obtains $k\lambda_D/D_s \gg 1$ and $dL/dt \approx 0.23$ m/s whereas the computational value is approximately 0.17 m/s. The first term of Eq. (17) yields $\Delta T_1 \approx 148$ K and the second term $\Delta T_2 \approx 24$ K, which gives $T_{\max}-T_g \approx 172$ K whereas the simulation gives $T_{\max}-T_g \approx 117$ K. This difference in estimated and simulated temperatures is due to the second term in Eq. (2), ($\propto$ grad T) which significantly inhibits C diffusion towards the SWNT edge. That is, the diffusion associated with the temperature gradient counteracts, in this case, that associated with the concentration gradient along the SWNT, and thereby decreases the resulting C flux to the growth edge. For conditions when analytical estimates are $T_{\max}-T_g<100$ K, the approximations given in Eqs. (17) and (18) have an acceptable accuracy (within 15–20 %).

B. Thermal restrictions of carbon NT growth

The temperature behavior during SWNT growth that is discussed above has important implications for physical evaporation techniques revealing (i) a high temperature restriction occurring under low inert gas pressure and (ii) a low temperature restriction occurring at high inert gas pressure.

First, the results presented in the preceding sections show that the SWNT temperature may be significantly higher than that of the ambient inert gas. Moreover, these results were obtained for a thermal accommodation coefficient of $\alpha=1/3$, which is the maximum value of α given that collisional energy transfer is restricted to the SWNT's radial direction. Accordingly, the value of α gives the lower limit for the temperature difference between the SWNT and the ambient gas. MD simulations of the ambient gas–SWNT heat exchange suggest that an additional atomic mass weight factor $(m_g/m_{\text{ref}})^{1/3}$ is present in heat exchange between the SWNT and gas molecules. Since this factor is less than one it leads to smaller values of h_g and, consequently, to larger values of temperature difference between the SWNT and the inert gas. To illustrate the effect of this factor, Fig. 6 shows simulation results calculated for the same set of parameters used for Fig. 3, but also includes this mass factor, which is $(m_g/m_{\text{ref}})^{1/3} \approx 0.3$ for He.

This factor significantly increases the difference between SWNT temperature and that of the gas and also the time required for SWNT cooling. Additionally, because of the initial increase in $T \approx 1700$ K the initial value for $\lambda_c \approx 0.04\,\mu$m and, therefore, the first stage (when the temperature is constant) is very short. There is very little time delay before the SWNT temperature decreases towards T_g. The influence of this mass factor may be explicitly estimated using analytical expressions obtained in the preceding section. For example, Fig. 7 shows the minimum possible difference between the SWNT and gas temperatures, $T-T_g$, corre-

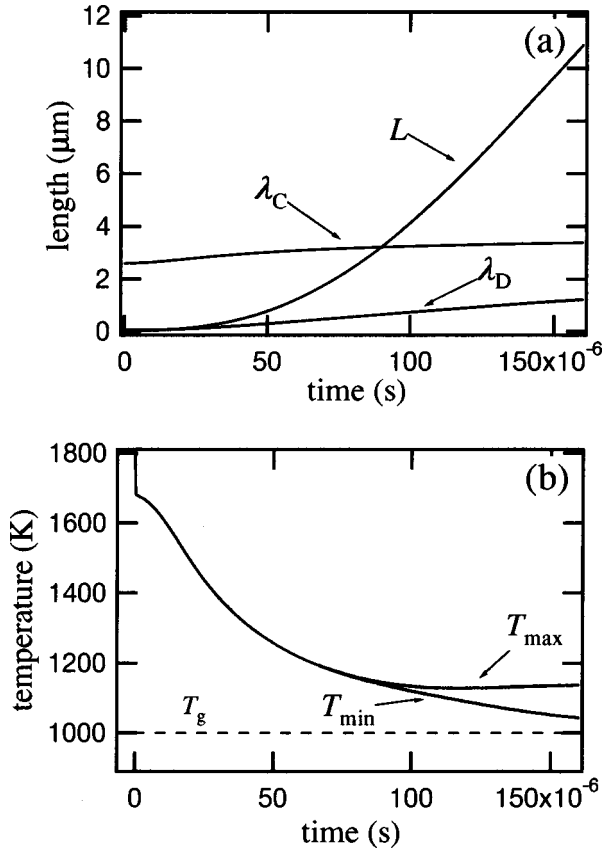

FIG. 6. Simulation results under the same conditions used for Fig. 3, but for $(m_g/m_{\mathrm{ref}})^{1/3}\approx 0.3$: (a) SWNT length together with SD and heat conductance lengths and (b) maximum and minimum temperatures.

sponding to the initial quasisteady state stage defined by Eq. (11) as a function of $P_c/\alpha P_g$ for the inert gases He, Ne, Ar, and Xe. The real temperature difference is obtained by inserting realistic values of α [Eq. (8)] into Eqs. (11) and (12). The graphs presented in Fig. 7 show that, even for very high ambient gas pressure (i.e., $P_c/\alpha P_g = 10^{-3}$), the maximum SWNT temperature may be more than 100 K higher than that of the gas.

The model developed here assumes that the temperature of the ambient gas is constant. However, condensation heat

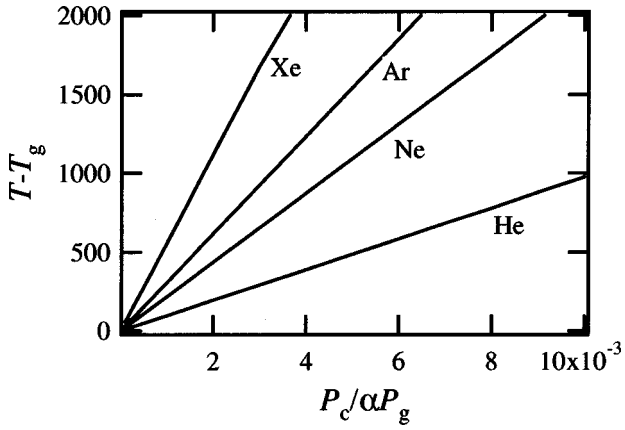

FIG. 7. Maximum temperature difference between the SWNT and the ambient gas as a function of $P_c/\alpha P_g$.

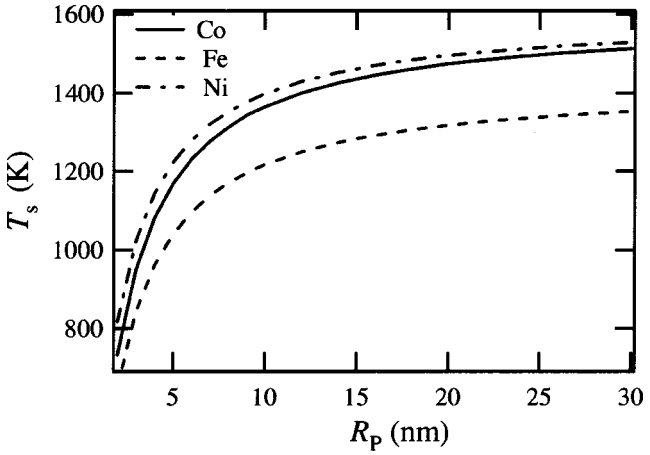

FIG. 8. Solidification temperature for eutectic C–Me composition as a function of metal particle radius.

release, which eventually dissipates into the ambient gas via SWNT–gas collisions, may increase the gas temperature. An increase in gas temperature T_g will increase the temperature of the growing NTs that will, in turn, affect the growth rates. For a vapor carbon atom density, N_c, the volumetric heat release of carbon condensation into CNTs will be $N_c(E_b + E_k)$, where $E_k \approx 0.3-0.5$ eV is the kinetic energy of the C atoms in the vapor at temperatures $T \approx 3000-5000$ K. This heat will be dissipated—via collisions—to the inert gas leading to increase in its temperature of $3N_g k_B \Delta T_g/2$ for monoatomic gases with volumetric density N_g. Using an expression for the gas density via the partial pressure one obtains

$$\Delta T_g \approx \frac{2}{3}\frac{P_c}{P_g}\frac{E_b+E_k}{k_B}. \tag{19}$$

This estimate yields $\Delta T_g \approx 60$ K for $P_g/P_c \approx 10^3$. In contrast, for $P_g/P_c \approx 10$ one has $\Delta T_g \approx 6000$ K. These values show that a high inert gas pressure ($\approx 10^4-10^5$ Pa) is required for CNT formation. At lower pressures the inert gas and C clusters become extremely hot stopping SWNT growth.

Second, the decrease in the SWNT temperature shown in Figs. 3, 4, and 6 suggest that this thermal mechanism is able to terminate SWNT growth, since the metal nanoparticle at the SWNT edge can solidify. That is, for the post-nucleation stages when the length of the carbon NT is much larger than the metal particle radius, the temperature of the metal nanoparticle is determined by the heat transfer over the SWNT surface, and the nanoparticle temperature is equal to that of the nanotube (because the contribution of metal particle surface in the total balance is negligibly small).

The simulations suggest that the growth termination may be due to this temperature decrease. This growth termination mechanism is consistent with the dependence of the solidification temperature, T_s, versus the nanoparticle radius that is shown for the C–Fe, C–Co, and C–Ni eutectics in Fig. 8. In particular, the data presented in Fig. 8 together with the temperature decrease shown in Fig. 6(b) shows that metal nanoparticles at SWNT ends are initially liquid and should solidify with time. For example, Fig. 6(b) shows that $T = 1200$ K at $t \approx 60\ \mu$s corresponds to the solidification tem-

perature of Ni nanoparticles with $R_p \approx 5$ nm, Co with $R_p \approx 6$ nm and Fe $R_p \approx 9$ nm. Metal nanoparticles with larger radii will also solidify, and solidification of the nanoparticle is able terminate the growth of SWNT due to a sharp decrease of the bulk diffusion coefficient of C through the particle. A typical value of bulk diffusion for liquid metals is $D_b \approx 10^{-5}\,\mathrm{cm}^2/\mathrm{s}$ whereas for solids it is $D_b \approx 10^{-8}\,\mathrm{cm}^2/\mathrm{s}$. Hence, the characteristic time of C diffusion through the Ni nanoparticle of $R_p \approx 5$ nm to the NT root is $\tau_d \approx R_p^2/D_b \approx 2.5\times 10^{-8}$ s when it is liquid, and $\tau_d \approx R_p^2/D_b \approx 2.5 \times 10^{-5}$ s after its solidification. For Co nanoparticle of $R_p \approx 6$ nm one has $\tau_d \approx R_p^2/D_b \approx 3.7\times 10^{-8}$ s for liquid and $\tau_d \approx R_p^2/D_b \approx 3.7\times 10^{-5}$ s for solid. Finally, for Fe nanoparticle of $R_p \approx 6$ nm one has $\tau_d \approx R_p^2/D_b \approx 8.3\times 10^{-8}$ s for liquid and $\tau_d \approx R_p^2/D_b \approx 8.3\times 10^{-5}$ s for solid state. In addition, the characteristic time of C impingement onto the nanoparticle surface from vapor at $P_c = 200$ Pa is $\tau_{\mathrm{imp}} \approx 1/(a_0^2 Q_c) \approx 2 \times 10^{-5}$ s. Thus, for the liquid nanoparticles one has $\tau_d \approx 2.5\text{–}8.3\times 10^{-8}\,\mathrm{s} \ll \tau_{\mathrm{imp}} \approx 2\times 10^{-5}$ s so that carbon atoms impinging onto the particle surface will diffuse to the SWNT root much faster than new carbon atom will impinge into the same surface sites. In contrast, when SWNT temperature decreases and the metal nanoparticles solidify, $\tau_d \approx 2.5\text{–}8.3 \times 10^{-5}$ s becomes higher than characteristic impingement time $\tau_{\mathrm{imp}} \approx 2\times 10^{-5}$ s. This means, that when the metal nanoparticle at SWNT tip freezes the impinging carbon atoms are no longer able to diffuse rapidly away from the particle surface, i.e., before new carbon atoms impinge at the same surface sites. This leads to C atom supersaturation at the metal nanoparticle surface causing precipitation directly on its surface, hence disabling SWNT growth. Also, Fig. 6 shows that small radii metal nanoparticles may remain liquid at temperatures lower than 1200 K, hence allowing carbon diffusion through the particles. However, low temperatures result in higher surface concentrations of adsorbed carbon on SWNT surfaces leading to nucleation of additional C layers and MWNT formation.

Once the metal nanoparticle surface is covered by precipitated carbon, additional carbon atoms impinging onto the particle and the SWNT surface cannot penetrate to the SWNT root. The surface concentration of adsorbed carbon rapidly increases to the adsorption–desorption equilibrium level defined by

$$n_{\mathrm{eq}} = Q_c \tau_a = \frac{P_c \exp(E_a/k_B T)}{v(2\pi m k_B T)^{1/2}}. \tag{20}$$

This occurs during the period $\delta t \approx \tau_a$. The SWNT temperature is the same as that of the gas during $\delta t \approx \tau^* \approx 5 \times 10^{-7}$ s. If the resulting C surface concentration at $T = T_g$ is too low to start the nucleation of a new CNT layer on surface, then the SWNT will be preserved and removed outside of the synthesis zone by gas flow. For the conditions shown in Fig. 3, the SWNT length will be about $L \approx 1.7\ \mu$m. On the other hand, if n_{eq} is sufficiently high to trigger new layer nucleation, then layer-by-layer MWNT formation will occur and will eventually result in the entrapment of the metal particle inside the MWNT structure.

It may be noted that, similarly to stage (i) of SWNT growth, C atoms that impinge on the outer layers of MWNTs will diffuse to the growth edge if the outer layer length is smaller than the SD length. Hence, all C atoms impinging onto the outer CNT surface diffuse to the layer edge and are incorporated into the wall. During this stage the heat release and also heat dissipation into the ambient inert gas are proportional to CNT length. Therefore, similarly to stage (i) of SWNT growth, the temperature of the MWNT wall is defined by the quasi-steady-state approximation of Eq. (11).

The proposed model allows us to comment on the experimental results of carbon nanostructure formation performed by laser ablation of graphite targets.[18,20] First, experimental study[18] shows that for Ar pressure in the range 0.1–100 Torr a carbon nanofoam consisting of a fractal-like web of randomly interconnected few nm radius carbon clusters forms at the substrate. Theoretical analysis[18] showed that these carbon clusters are formed by carbon atom collisions in vapor. Our model additionally suggests that under these Ar pressures the temperature of carbon nanostrutures (NTs) assembled by the impinging carbon atoms should increase to a temperature above the temperature of graphite sublimation ($\approx$4000 K). This means that during the assembly in vapor, carbon nanostuctures should disintegrate back into smaller fragments and, in fact, can assemble into larger structures only when they reach a solid substrate where the condensation heat may be easily dissipated by heat conduction into the solid. Thus, we suggest that in addition to the collision rate of C atoms the dimensions of carbon nanoclusters forming this foam is also controlled by thermal effects including condensation heat release and heat dissipation to the inert gas. Second, our model exhibits good qualitative agreement with temperature measurements of carbon particles in pulsed laser synthesis, which shows a plateau stage.[20] In fact, temperature measurements performed in this work show that the cooling of carbon clusters from the initial temperature to that of the inert gas requires several milliseconds. Our simulations given in Figs. 3, 4, and 6 show that cooling requires 0.1–0.15 ms. Notwithstanding the fact that the power dependence of heat exchange on atomic mass given in Fig. 2 suggests that heat exchange per one Ar atom collision is about 2 times more effective than that of a He atom a more detailed analysis shows that cooling time for the parameters of the experiment case[20] should be larger. This is because, first, our temperature simulation given in Fig. 6 is done for He at 10^5 Pa whereas experiments are done for Ar at 500 Torr ($6.6\,10^4$ Pa). Second, $m_{\mathrm{Ar}}/m_{\mathrm{He}} \approx 10$ and Eq. (7) suggests that for the same pressure He provides 3.3 times more collisions per surface area unit. Thus, the resulting number ($1.5\times 3.3/2$) suggests that for the simulation shown in Fig. 6 the heat exchange coefficient is about 2.5 times larger and the cooling time consequently 2.5 times shorter than that for Ar at 500 Torr. The remaining discrepancy may be attributed to a wide range of surface microenergetic parameters depending on SWNT radius and chirality[39,41,42] and also to a number of physical effects of pulsed laser synthesis neglected in our study, such as heating of the inert gas near the evaporated target due to very high initial kinetic energies that the carbon atoms may have after pulsed laser evaporation.

IV. SUMMARY AND CONCLUSIONS

The growth of carbon nanotubes is a complicated process involving many effects and characterized by many restrictions. One of the main parameters defining growth kinetics is the growth temperature. The temperature of the growing nanotube is defined by a set of interacting parameters for condensation heat release and heat dissipation from the nanotube surface.

Our study provides a set of coupled growth kinetics—thermal physics phenomenological equations that are numerically solvable, as well as explicit analytical estimates giving values of SWNT temperatures during growth. We also provide the main results of a molecular dynamics study characterizing heat exchange between the SWNT and inert ambient gases. Our study, combining in a simulation phenomenological and MD models shows that the SWNT temperature may be significantly different from that of the inert gas, and a high pressure of the inert gas is shown to inhibit an uncontrollable increase in the temperature of assembling C nanoclusters. This model also shows that the temperature of SWNTs growing from the vapor has a complicated behavior and may have various stages.

The highest temperature of the SWNT during the entire growth process is found during the initial stage. During this stage the SWNT is shorter than the surface diffusion length of C atoms adsorbed on the SWNT wall, and both heat release and heat dissipation are proportional to the SWNT length. Thus, the temperature of the SWNT (i) remains constant during growth, (ii) is uniform over the entire length of the carbon NT, and (iii) may be significantly higher than that of the inert gas. Even for inert gas pressures used in SWNT synthesis, i.e., 10^4-10^5 Pa, this difference may be several hundreds of Kelvin. After this stage, i.e., when the SWNT becomes longer than the SD length, the temperature decreases towards that of the ambient gas. The temperature of the SWNT remains uniform over the length of the SWNT, as long as the tube is shorter than the characteristic heat conductance length. The SWNT cooling rate depends critically on the efficiency of SWNT–gas collisional energy transfer, which our MD simulations show is larger for heavier gas atoms. The simulations also reveal that efficient energy transfer occurs only in the tube radial direction. After this stage the temperature distribution along the SWNT is no longer uniform. However, this temperature gradient along the length of the carbon NT is significant only if the SWNT temperature remains significantly higher than that of the gas (if, for example, the SWNT–gas collisional energy transfer is not efficient). Our estimates also suggest that the decrease in temperature which occurs after the first stage may terminate SWNT growth. This occurs since the metal nanoparticle at the end of the SWNT solidifies which, in turn, significantly decelerates C diffusion to the SWNT root through the metal nanoparticle. This also results in carbon precipitation on the metal particle surface, disabling it from continuing the growth process. At this stage nucleation of outer carbon layers may lead to the formation of MWNTs with metal nanoparticles entrapped in the MWNT structure. This mechanism may limit the SWNT length during growth from the vapor.

It should also be noted that the model developed in this work, which includes many microcsopic surface kinetic parameters, may be readily coupled with macroscopic continuum gas flow dynamics models combined with heat and mass transfer, allowing one to investigate the effect of gas flow on carbon NT growth and to investigate more complicated growth modes occurring when parameters such as carbon vapor pressure, inert gas pressure, and temperature change with time. This model may be also extended to include (i) specific features of carbon NT growth that are found in arc discharge plasma and other growth techniques, (ii) new features of surface kinetics associated with electric field effects, and (iii) the involvement of carbon dimers and larger aggregates in the growth process.

ACKNOWLEDGMENTS

The authors are very grateful to Dr. A. Krasheninnikov and co-workers from the University of Helsinki (Finland) for providing them with new microenergetics results prior to their publication.[42] The authors would also like to thank Professor D. Tománek from The Michigan State University (USA) for stimulating discussions on the subject of this work. Two of the authors (K.B. and A.R.) are grateful for financial support from the Swedish Foundation for Strategic Research.

[1] A. Oberline, M. Endo, and T. Koyama, J. Cryst. Growth **32**, 335 (1976).
[2] R. T. K. Baker and P. S. Harris, in *Chemistry and Physics of Carbon*, edited by P. L. Walker, Jr. and P. A. Thrower (Deker, New York, 1978), pp. 83–161, and references therein.
[3] G. G. Tibbetts, J. Cryst. Growth **66**, 632 (1984).
[4] S. Iijima, Nature (London) **354**, 56 (1991).
[5] S. Iijima, P. M. Ajayan, and T. Ichihashi, Phys. Rev. Lett. **69**, 3100 (1992).
[6] T. W. Ebbesen and P. M. Ajayan, Nature (London) **358**, 220 (1992).
[7] P. M. Ajayan, Prog. Cryst. Growth Charact. Mater. **38**, 37 (1997).
[8] S. Iijima, Mater. Sci. Eng., B **B19**, 172 (1993).
[9] X. F. Zhang, X. B. Zhang, G. Van Tendeloo, S. Amelinckx, M. Op de Beeck, and J. Van Landuyt, J. Cryst. Growth **130**, 368 (1993).
[10] S. Amelinckx, X. B. Zhang, D. Bernaerts, X. F. Zhang, V. Ivanoy, and J. B. Nagy, Science **265**, 63 (1994).
[11] R. E. Smalley, Mater. Sci. Eng., B **B19**, 1 (1993).
[12] M. Endo, K. Takeuchi, S. Igarashi, K. Kobori, M. Shiraishi, and H. W. Kroto, J. Phys. Chem. Solids **54**, 1841 (1993).
[13] E. G. Gamally and T. W. Ebbesen, Phys. Rev. B **52**, 2083 (1995).
[14] A. Thess, R. Lee, P. Nikolaev *et al.*, Science **273**, 483 (1996).
[15] H. Lange, A. Huczko, M. Sioda, and O. Louchev, J. Nanoscience Nanotechnology **3**, 51 (2003).
[16] A. Gorbunov, O. Jost, W. Pompe, and A. Graff, Carbon **40**, 113 (2002); Appl. Surf. Sci. **197–198**, 464 (2002).
[17] E. Gamaly, A. V. Rode, W. K. Maser, E. Munoz, A. M. Benito, M. T. Martinez, and G. G. de la Fuente, Appl. Phys. A: Mater. Sci. Process. **A70**, 161 (2000); **A69**, S121 (1999).
[18] A. V. Rode, E. G. Gamaly, and B. Luther-Davies, Appl. Phys. A: Mater. Sci. Process. **A70**, 135 (2000).
[19] A. A. Puretzky, D. B. Geohagen, X. Fan, and S. J. Pennycook, Appl. Phys. Lett. **76**, 182 (2000); Appl. Phys. A: Mater. Sci. Process. **A70**, 153 (2000).
[20] A. A. Puretzky, H. Schittenhelm, X. Fan, M. J. Lance, L. F. Allard, Jr., and D. B. Geohegan, Phys. Rev. B **65**, 245425 (2002).
[21] M. Yudasaka, R. Kikuchi, T. Matsui, Y. Ohki, S. Yoshimura, and E. Ota, Appl. Phys. Lett. **67**, 2477 (1995).
[22] M. Yudasaka, T. Komatsu, T. Ichihashi, Y. Achiba, and S. Iijima, J. Phys. Chem. B **102**, 4892 (1998).
[23] E. Munoz, W. K. Mazer, A. M. Benito, M. T. Martinez, G. F. de la Fuente, A. Righi, J. L. Sauvajol, E. Anglaret, and Y. Maniette, Appl. Phys. A: Mater. Sci. Process. **A70**, 145 (2000).
[24] S. Bandow, S. Asaka, Y. Saito, A. M. Rao, L. Grigorian, E. Richter, and P. C. Eklund, Phys. Rev. Lett. **80**, 3779 (1998).
[25] P. Zhang and V. H. Crespi, Phys. Rev. Lett. **83**, 1791 (1999).

[26] M. Volpe and F. Cleri, J. Chem. Phys. **115**, 3308 (2001).
[27] T. Kawai, Y. Miyamoto, O. Sugino, and Y. Koga, Phys. Rev. B **66**, 033404 (2002).
[28] J. Gavillet, A. Loiseau, C. Journet, F. Willaime, F. Ducastelle, and J.-C. Charlier, Phys. Rev. Lett. **87**, 275504 (2001).
[29] X. Fan, R. Buczko, A. A. Puretzky, D. B. Geohegan, J. Y. Howe, S. T. Pantelides, and S. J. Pennycook, Phys. Rev. Lett. **90**, 145501 (2003).
[30] J. R. Hester and O. A. Louchev, Appl. Phys. Lett. **80**, 2580 (2002); O. A. Louchev and J. R. Hester, J. Appl. Phys. **94**, 2002 (2003), and references therein.
[31] O. A. Louchev, Y. Sato, and H. Kanda, J. Appl. Phys. **91**, 10074 (2002).
[32] O. A. Louchev, Y. Sato, and H. Kanda, Phys. Rev. E **66**, 011601 (2002).
[33] O. A. Louchev, T. Laude, Y. Sato, and H. Kanda, J. Chem. Phys. **118**, 7622 (2003).
[34] O. A. Louchev and Y. Sato, Appl. Phys. Lett. **74**, 194 (1999).
[35] O. A. Louchev, Y. Sato, and H. Kanda, J. Appl. Phys. **89**, 3438 (2001).
[36] E. F. Kukovitsky, S. G. L'vov, and N. A. Sainov, Mol. Mater. **10**, 165 (1998).
[37] E. F. Kukovitsky, S. G. L'vov, and N. A. Sainov, Chem. Phys. Lett. **317**, 65 (2000).
[38] E. F. Kukovitsky, S. G. L'vov, N. A. Sainov, V. A. Shustov, and L. A. Chernozatonskii, Chem. Phys. Lett. **355**, 65 (2000).
[39] Y. H. Lee, S. G. Kim, and D. Tománek, Phys. Rev. Lett. **78**, 2393 (1997).
[40] Y.-K. Kwon, Y. H. Lee, S. G. Kim, P. Jund, D. Tománek, and R. E. Smalley, Phys. Rev. Lett. **79**, 2065 (1997).
[41] N. Kitamura and A. Oshiyama, J. Phys. Soc. Jpn. **70**, 1995 (2001).
[42] A. V. Krasheninnikov, K. Nordlund, P. O. Lehtinen, A. S. Foster, A. Ayuela, and R. M. Nieminen, Phys. Rev. B **69**, 073402 (2004).
[43] K. Bolton and A. Rosén, Phys. Chem. Chem. Phys. **4**, 481 (2002).
[44] K. Bolton and S. Gustavsson, Chem. Phys. **291**, 161 (2003).
[45] F. Kokai, K. Takahashi, M. Yudasaka, R. Yamada, T. Ichihashi, and S. Iijima, J. Phys. Chem. B **103**, 4346 (1999).
[46] F. Kokai, K. Takahashi, D. Kasuya, M. Yudasaka, and S. Iijima, Appl. Phys. A: Mater. Sci. Process. **A73**, 401 (2001).
[47] C. J. Brabec, A. Maiti, C. Roland, and J. Bernholc, Chem. Phys. Lett. **236**, 150 (1995).
[48] A. Maiti, C. J. Brabec, C. M. Roland, and J. Bernholc, Phys. Rev. Lett. **73**, 2468 (1994).
[49] J. Ch. Charlier, X. Blase, A. De Vita, and R. Car, Appl. Phys. A: Mater. Sci. Process. **A68**, 276 (1999).
[50] X. Blase, J.-C. Charlier, A. De. Vita *et al.*, Phys. Rev. Lett. **83**, 5078 (1999).
[51] A. Maiti, C. J. Brabec, C. M. Roland, and J. Bernholc, Phys. Rev. Lett. **73**, 2468 (1994).
[52] A. Maiti, C. J. Brabec, C. Roland, and J. Bernholc, Phys. Rev. B **52**, 14850 (1995).
[53] J. C. Charlier, A. De Vita, X. Blase, and R. Car, Science **275**, 646 (1997).
[54] M. B. Nardelli, C. Brabec, A. Maiti, C. Roland, and J. Bernholc, Phys. Rev. Lett. **80**, 313 (1998).
[55] D. H. Robertson, D. W. Brenner, and J. M. Mintmire, Phys. Rev. B **45**, 12592 (1992).
[56] N. Park, K. Lee, S. Han, J. Yu, and J. Ihm, Phys. Rev. B **65**, 121405(R) (2002).
[57] Y. Shibuta and S. Maruyama, Physica B **323**, 187 (2002).
[58] J. Tersoff, Phys. Rev. Lett. **61**, 2879 (1988); Phys. Rev. B **37**, 6991 (1988).
[59] D. V. Brenner, Phys. Rev. B **42**, 9458 (1990).
[60] K. Nordlund, J. Keinonen, and T. Matilla, Phys. Rev. Lett. **77**, 699 (1996).
[61] J. P. Lu and W. Yang, Phys. Rev. B **49**, 11421 (1994).
[62] B. I. Henri and M. T. Batchelor, Phys. Rev. E **68**, 016112 (2003).
[63] Sum of the binding energy, $E_b = 7.3$ eV, and the kinetic energy, which is $\ll E_b$ for conditions when inert gas pressure is high enough to effectively dissipate excessive kinetic energy that carbon atoms may have after evaporation.
[64] Y. S. Touloukian, *Thermophysical Properties of Matter* (Plenum, New York, 1970), Vol. II, p. 41.
[65] C. N. Hinshelwood, Proc. R. Soc. London, Ser. A **113**, 230 (1927).
[66] S. Nordholm, L. E. B. Börjesson, L. Ming, and H. Svedung, Ber. Bunsenges. Phys. Chem. **101**, 574 (1997).
[67] V. Celli, D. Himes, P. Tran, J. P. Toennies, C. H. Wöll, and G. Zhang, Phys. Rev. Lett. **66**, 3160 (1991).